

Nonlinear radiation pressure dynamics in an optomechanical crystal

Alex G. Krause,^{1,2} Jeff T. Hill,^{1,2,3} Max Ludwig,⁴ Amir H. Safavi-Naeini,^{1,2,3}
Jasper Chan,^{1,2} Florian Marquardt,^{4,5} and Oskar Painter^{1,2,*}

¹*Kavli Nanoscience Institute and Thomas J. Watson, Sr.*

Laboratory of Applied Physics, California Institute of Technology, Pasadena, CA 91125

²*Institute for Quantum Information and Matter, California Institute of Technology, Pasadena, CA 91125*

³*Edward L. Ginzton Laboratory, Stanford University, Stanford, CA 94305*

⁴*Institute for Theoretical Physics, Universität Erlangen-Nürnberg, 91058 Erlangen*

⁵*Max Planck Institute for the Science of Light, Günther-Scharowsky-Straße 1/Bau 24, D-91058 Erlangen, Germany*

(Dated: December 3, 2024)

Utilizing a silicon nanobeam optomechanical crystal, we investigate the attractor diagram arising from the radiation pressure interaction between a localized optical cavity at $\lambda_c = 1552$ nm and a mechanical resonance at $\omega_m/2\pi = 3.72$ GHz. At a temperature of $T_b \approx 10$ K, highly nonlinear driving of mechanical motion is observed via continuous wave optical pumping. Introduction of a time-dependent (modulated) optical pump is used to steer the system towards an otherwise inaccessible dynamically stable attractor in which mechanical self-oscillation occurs for an optical pump red-detuned from the cavity resonance. An analytical model incorporating thermo-optic effects due to optical absorption heating is developed, and found to accurately predict the measured device behavior.

The field of optomechanics, concerned with the interaction of an optical cavity and a mechanical resonator [1], has been of recent interest for its promise for use in sensors [2, 3], nonlinear optics [4, 5], and demonstrations of macroscopic quantum mechanics [6, 7]. To lowest order, the mechanical displacement linearly modulates the frequency of the optical resonance in a cavity-optomechanical system. This, however, gives rise to an inherently nonlinear phase modulation, and through radiation-pressure backaction on the mechanical element, yields nonlinear system dynamics [8]. Much of the previous work has focused on the linearized regime where the interaction with the optical field still gives rise to a host of interesting phenomena such as a modified spring constant [9], damping or amplification of the mechanics [10], and EIT-like slow-light effects [11, 12]. Recently, several experiments have pushed into the quantum regime using back-action cooling and damping in the linearized regime to damp nanomechanical resonators to near their quantum ground state of motion [13, 14].

In this work, we instead demonstrate new features and tools in the nonlinear regime of large mechanical oscillation amplitude. Previous experimental works have shown that a blue-detuned laser drive can lead to stable mechanical self-oscillations [15–18], or even chaotic motion [19]. Theoretical predictions of an intricate multistable attractor diagram [8] have so far eluded experimental observation, except for the elementary demonstration of dynamical bistability in a photothermally driven system [20]. In the present work, we are able to verify the predicted attractor diagram and further utilize a modulated laser drive to steer the system into an isolated high-amplitude attractor. This introduces pulsed control of nonlinear dynamics in optomechanical systems dominated by radiation pressure backaction, in analogy to what has been

shown recently for a system with an intrinsic mechanical bistability [21].

We employ a one-dimensional (1D) optomechanical crystal (OMC) designed to have strongly interacting optical and mechanical resonances [22]. We fabricate this nano-scale structure from a free-standing silicon beam by etching into it a periodic array of holes which act as Bragg mirrors for both acoustic and optical waves [23]. By perturbing this periodicity, a central defect region is created which co-localizes optical modes designed to fall in the telecommunications band ($\lambda_c \approx 1550$ nm), and acoustic modes in the microwave band ($\omega_m/2\pi \approx 4$ GHz). A scanning electron micrograph (SEM) of the beam is shown in Fig. 1a along with finite element method (FEM) simulations of the optical (Fig. 1b) and mechanical (Fig. 1c) modes. To reduce radiation of the mechanical energy into the bulk, the OMC is surrounded by a periodic ‘cross’ structure which has a full acoustic bandgap around the mechanical frequency (Fig. 1a, green overlay) [24].

The experimental setup is shown schematically in Fig. 1d. The silicon chip containing the device is placed into a helium flow cryostat where it rests on a cold finger at $T \approx 4$ K (the temperature of the device in this set-up is estimated to be $T_b \approx 10$ K). Input laser light is sent into the device via a tapered optical fiber, which, when placed in the near-field of the device, evanescently couples to the optical resonance of the OMC [25]. The transmitted light is detected on a high-frequency photodiode (D1) connected to a real-time spectrum analyzer (RSA). We also employ an electro-optic modulator (EOM) in the laser’s path to resonantly drive the mechanical resonator. Finally, we can send in a low-power, counter-propagating probe laser whose detected spectrum (D2) is fit to independently measure the mechanical amplitude and the pump-cavity detuning.

Utilizing this setup, we determine that the optical resonance is at $\lambda_c = 1542$ nm with intrinsic damping rate $\kappa_i/2\pi = 580$ MHz, giving $Q_{c,i} = 3.3 \times 10^5$. However, due to the large

*Electronic address: opainter@caltech.edu; URL: <http://copilot.caltech.edu>

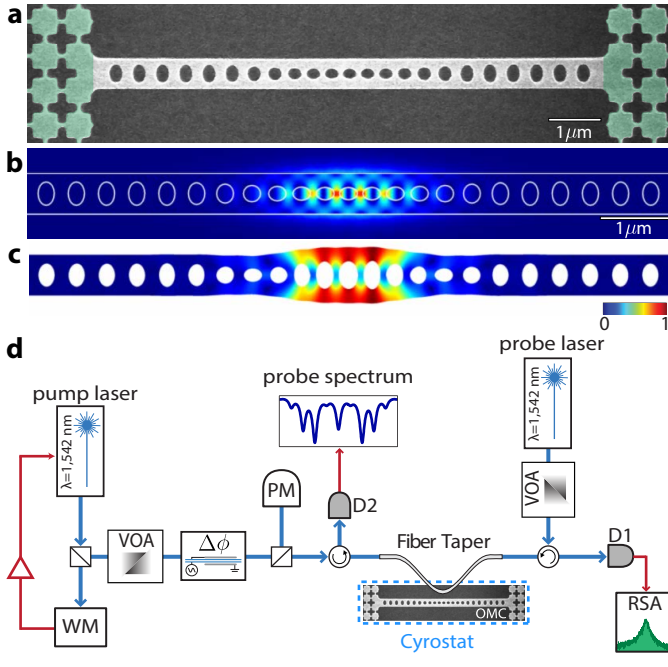


FIG. 1: (a) SEM of the optomechanical nanobeam surrounded by phononic shield (green). (b) FEM-simulated electromagnetic energy density of first-order optical mode; white outline denotes edges of photonic crystal. (c) FEM-simulated mechanical mode profile (displacement exaggerated). In (b) the colorscale bar indicates large (red) and small (blue) energy density, whereas in (c) the scale bar indicates large (red) and small (blue) displacement amplitude. (d) Simplified schematic of experimental setup. WM: wavemeter, $\Delta\phi$: electro-optic phase modulator, OMC: optomechanical crystal, D1: pump light detector, D2: probe detector, VOA: variable optical attenuator, PM: power meter

coupling to the taper, the total decay rate is $\kappa/2\pi = 1.7$ GHz, with $Q_c = 1.2 \times 10^5$. The mechanical mode is found to be at $\omega_m/2\pi = 3.72$ GHz damped at rate $\gamma_i/2\pi = 24$ kHz, with $Q_m = 1.55 \times 10^5$. For this experiment cryogenic temperatures are needed because the room-temperature mechanical quality-factor is much lower, $Q_m \approx 2 \times 10^3$, requiring such high optical powers that heating effects would obscure the signatures of the radiation-pressure nonlinearity.

The coupling of the optical resonance frequency to the mechanical displacement yields the interaction Hamiltonian, $H_{\text{int}} = \hbar g_0 \hat{a}^\dagger \hat{a} \hat{x}$ where \hat{a} (\hat{x}) is the optical (mechanical) field amplitude, g_0 is the bare coupling rate and \hbar is Planck's constant over 2π . The physical mechanical displacement is related to the field operator by $x = x_{\text{zpf}} \langle \hat{x} \rangle$ where the zero-point amplitude of the resonator is $x_{\text{zpf}} = (\hbar/2m_{\text{eff}}\omega_m)^{1/2} = 2.7$ fm, using the effective motional mass as determined through FEM-simulation, $m_{\text{eff}} = 311$ fg. Utilizing a calibration of the per-photon cooling power [13] we find that $g_0/2\pi = 941$ kHz. These device parameters put our system well into the sideband resolved regime $\kappa/\omega_m \ll 1$, but far from that of single-photon strong-coupling, $g_0/\kappa \gtrsim 1$ which is necessary for many quantum protocols.

The classical nonlinear optomechanical equations of motion

for the mechanical displacement (x) and the optical amplitude ($a = \langle \hat{a} \rangle$) are

$$\ddot{x}(t) = -\gamma_i \dot{x}(t) - \omega_m^2 x(t) + 2\omega_m g_0 x_{\text{zpf}} |a(t)|^2, \quad (1)$$

$$\dot{a}(t) = \left[-\frac{\kappa}{2} + i \left(\Delta_L + \frac{g_0}{x_{\text{zpf}}} x(t) \right) \right] a(t) + \sqrt{\frac{\kappa_e}{2}} a_{\text{in}}, \quad (2)$$

where the strength of the input drive laser at frequency ω_L with total power P_{in} is given by $a_{\text{in}} = \sqrt{P_{\text{in}}/\hbar\omega_L}$ which is coupled in at rate $\kappa_e/2$, and detuned relative to the cavity frequency, ω_c , by $\Delta_L = \omega_L - \omega_c$. Since we are interested in the regime of self-sustained oscillations, where the motion of the oscillator is coherent on time scales much longer than the cavity lifetime, we can take the mechanical motion to be sinusoidal with amplitude A , $x(t) = A \sin \omega_m t$. This allows us to solve for the optical field as,

$$a(t) = \sqrt{\frac{\kappa_e}{2}} a_{\text{in}} e^{i\Phi(t)} \sum_n i^n \alpha_n e^{in\omega_m t}, \quad (3)$$

where $\Phi(t) = -\beta_m \cos \omega_m t$ and $\alpha_n = J_n(\beta_m) / (\kappa/2 + i(n\omega_m - \Delta_L))$. Here J_n is the Bessel function of the first kind, n -th order, and its argument is the unitless modulation strength $\beta_m = (A g_0) / (x_{\text{zpf}} \omega_m)$. For $\beta_m \ll 1$ only the terms oscillating at the mechanical frequency, ω_m , are appreciable, so the interaction can be linearized, and only the first-order radiation pressure terms are present. However, for $\beta \geq 1$ the higher harmonic terms at each $n\omega_m$ have significant amplitude and also exert backaction forces which can dominate the first-order component.

The thermal amplitude is too small to enter the nonlinear regime in our devices ($\beta_{\text{th}} \approx 0.01$), however, a laser positively detuned from the cavity, or external laser modulation, can provide amplification to drive the mechanics into the high- β regime. This leads to a rich amplitude and detuning dependent gain spectrum, which can be solved for [8] by calculating the energy lost in one mechanical cycle from friction $P_{\text{fric}} = m_{\text{eff}} \gamma_i \langle \dot{x}^2 \rangle$ and comparing it to that gained (or lost) from the optical radiation force $P_{\text{rad}} = (\hbar g_0 / x_{\text{zpf}}) \langle |\hat{a}|^2 \dot{x} \rangle$ across a sweep of amplitude/detuning pairs (β_m, Δ_L).

This calculation for our system parameters generates the plot shown in Fig. 2a where the color indicates the ratio of these terms (more precisely, $P_{\text{rad}}/P_{\text{fric}} - 1$) at a laser input power of $P_{\text{in}} = 151$ μW. Finally, imposing energy conservation, $P_{\text{rad}}/P_{\text{fric}} = +1$, yields the steady-state solution contours as shown in Fig. 2a. Although the entire contour is a physical solution, the equilibrium is only stable when the power ratio decreases upon increasing the mechanical amplitude, $\frac{\partial}{\partial \beta} \frac{P_{\text{rad}}}{P_{\text{fric}}} < 0$ (i.e. stability is found at the 'tops' of the contours) [8]. It is seen that at the highest powers (Fig. 2a, black curve) for most detunings there are multiple possible mechanical amplitude solutions, β_m .

In the device studied here, there is also a small frequency shift of the optical cavity caused by heating due to material ab-

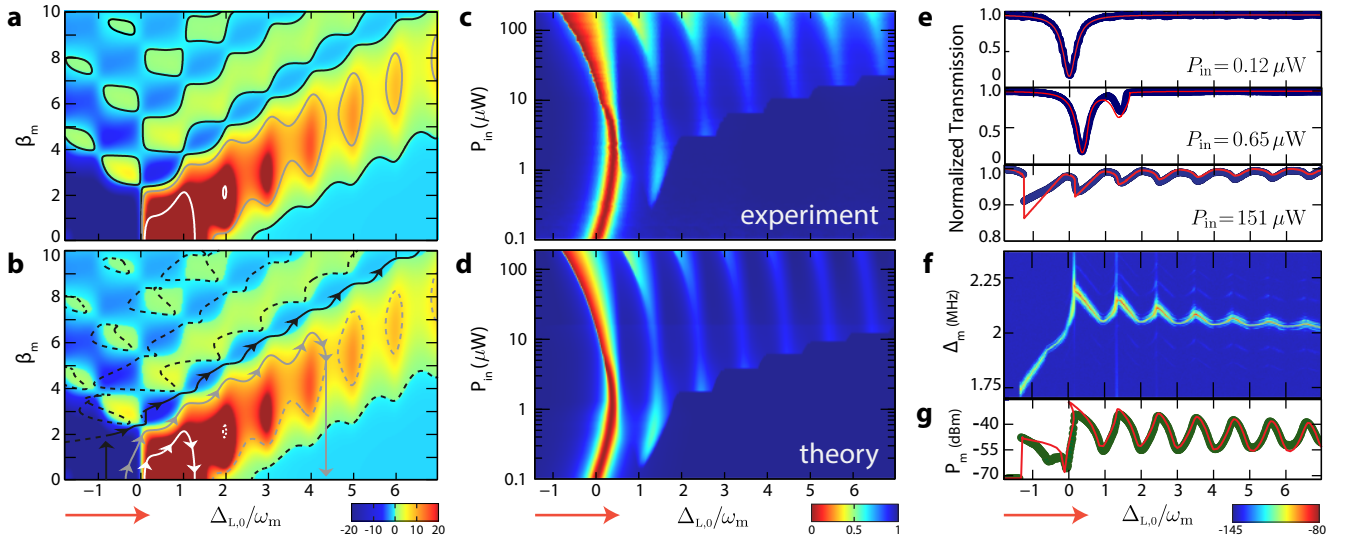


FIG. 2: (a) Calculated gain spectrum for the OMC in the amplitude-detuning plane. Color scale indicates ratio of power input to that lost from friction ($P_{\text{rad}}/P_{\text{fric}} - 1$) at $P_{\text{in}} = 151 \mu\text{W}$. Positive values are regions of mechanical self-oscillation. Curves indicate power-conserving solution contours at selected input powers: $0.65 \mu\text{W}$ (white), $6.5 \mu\text{W}$ (grey), $151 \mu\text{W}$ (black). (b) same as (a), with contours now shifted by estimated thermo-optic effects, where solid lines indicate the path taken by the mechanical oscillator during laser sweep for same powers as in (a). Dashed lines are contours which are either unstable or unreachable by a slow sweep of laser detuning. Red arrows indicate direction of laser scan. (c) Plot of device transmission spectrum for a series of laser powers. Scans are scaled at each power to span the range $0 - 1$. Stair-step shape indicates onset of self-oscillation due to progressively higher-order sidebands. (d) Theoretical calculation of (c), with the optical cavity shift per-photon, c_{to} , as the only free parameter. (e) Plots of normalized transmission from scans in (c) at $P_{\text{in}} = 0.12 \mu\text{W}$ (top), $0.65 \mu\text{W}$ (center), $151 \mu\text{W}$ (bottom), (blue data) with theoretical curve overlaid (red). (f) Power spectral density of detected signal near the mechanical frequency for $P_{\text{in}} = 151 \mu\text{W}$, showing frequency shifts of the mechanical mode, Δ_m , from its bare frequency, $\omega_m/2\pi = 3.72 \text{ GHz}$. Color scale is detected power density in dBm/Hz. (g) Total integrated power of spectra in (f), green circles, with theoretical model (red curve). An over-all scale-factor is the only free parameter. Due to a small drift in the center frequency of the optical cavity, the highest power scan in (e) and corresponding scans in (f)-(g) are red-shifted relative to the same power in (c)-(d)

sorption of the intracavity photons. This heating is slow relative to the other time-scales in the system, but fast compared to our laser scan speed, and can be modeled as an effective blue-shift of the laser detuning proportional to $\Delta_{L,0} = \Delta_L - c_{\text{to}}\bar{n}_a$, where the per photon thermo-optic frequency shift of the optical cavity is measured to be $c_{\text{to}}/2\pi = -216 \text{ kHz}$, and \bar{n}_a is the estimated average photon number [13] for each (β_m, Δ_L) . Including this effect, the shifted contours are shown in Fig. 2b for their respective input powers. The solid lines with arrows indicate the expected path traversed by the mechanical resonator during a slow (adiabatic) laser scan from lower to higher laser frequency (left to right) at each power. The dashed lines are contours that are either unstable, or unreachable by this adiabatic laser sweep.

We first explore the attractor diagram by measuring the system dynamics as the oscillator traverses this lowest-lying contour, for a range of powers. Since we are monitoring the transmission of a double-sided optical cavity, a dip in transmission is seen when scanning through the cavity resonance, indicating that light is entering the cavity and being lost to absorption or scattering. At low powers one sees a single dip ($P_{\text{in}} < 0.3 \mu\text{W}$, in Fig. 2c and top plot in Fig. 2e). Upon increasing the laser power, optomechanical dynamical backaction effects start to drive the system, and beyond threshold there is self-oscillation of the mechanical element. When this occurs, a large frac-

tion of the optical photons are now scattered, which results in a second dip of the transmission near the first mechanical sideband ($\Delta_{L,0}/\omega_m = 1$) in Fig. 2c. As the power is increased, the self-oscillation threshold is achieved for detunings at progressively higher mechanical sidebands, $\Delta = n\omega_m$, resulting in the stair-step behavior observed in the transmission. Physically, mechanical oscillations at the n -th sideband detuning are generated by a multi-photon gain process involving n photon-phonon scattering events. As mentioned, the overall red-shift of the curves at the highest powers, is due to the thermo-optic effect. We present our theoretically expected transmission spectra in Fig. 2d and find good agreement.

More information about the state of the mechanical oscillator can be gained by recording the spectrum of the signal near the mechanical frequency as shown in Fig. 2f for the highest power transmission scan of Fig. 2e. We note that backaction effects blue-shift the resonator frequency by an appreciable amount ($\sim 2 \text{ MHz}$) from its intrinsic value of $\omega_m/2\pi = 3.7 \text{ GHz}$. This frequency shift, Δ_m , depends on the laser detuning in a more intricate fashion than a linear calculation of the optical spring effect would suggest. A measure of oscillation amplitude can be extracted from the total power in this mechanical sideband, and its dependence on detuning is shown in Fig. 2f. Although the mechanical amplitude β_m increases monotonically with detuning, we observe that the to-

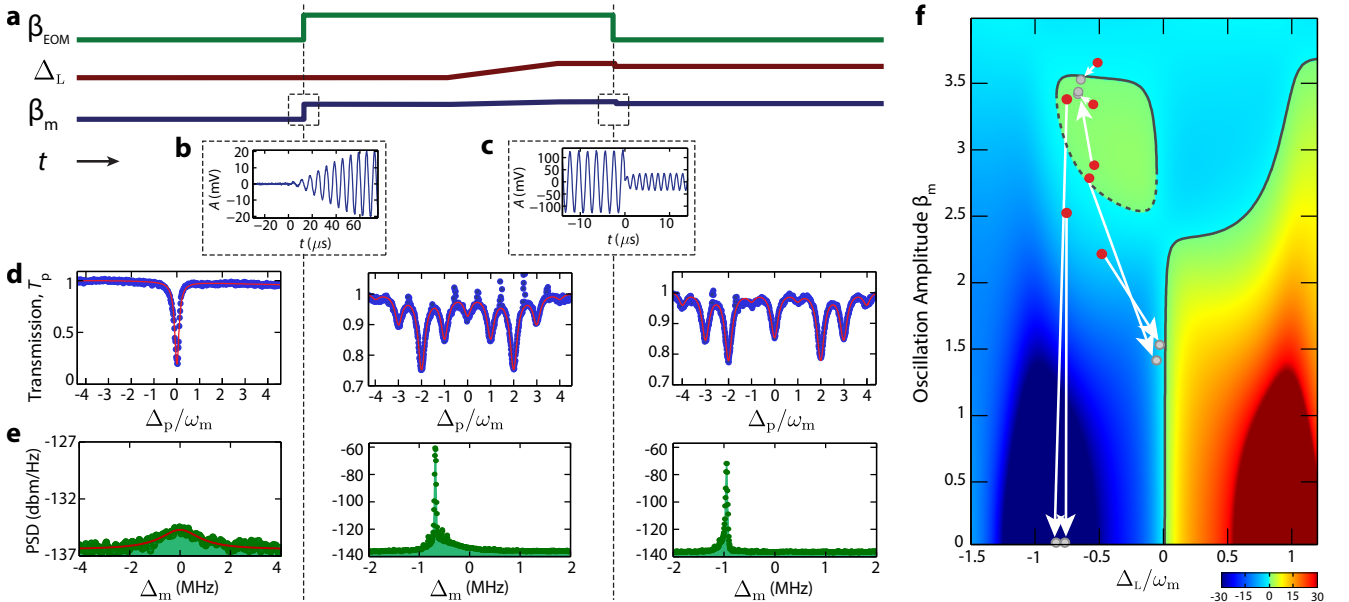


FIG. 3: (a) Schematic of state preparation scheme including change in the two control parameters, modulation drive strength (β_{EOM}) and laser-cavity detuning (Δ_L), along with the resulting oscillator amplitude (β_m). (b) Time-signal of one quadrature of detected mechanical amplitude during the turn-on of the EOM drive at $t = 0$, showing amplitude ring-up. For clarity, the signal is mixed down from the mechanical frequency carrier at 3.7 GHz to 150 kHz. (c) same as (b) with modulation turned off at $t = 0$ for a case where the system remained trapped in high-amplitude state; carrier mixed down to 500 kHz. (d) Transmission scans of the low-power probe laser (blue data points) with with the fit curves (red) used to extract (β_m, Δ_L) during each period of sequence, $\Delta_p = \omega_p - \omega_c$ with ω_p the probe frequency. (e) Mechanical power spectrum (green data) near the mechanical frequency during these periods. In the left panel the resonator is in a cooled thermal state and the red-line is a fit used to extract mechanical parameters. (f) Plot of the normalized gain spectrum in the detuning-amplitude plane with overlaid stable solution contour (black solid curve) at $P_{\text{in}} = 43 \mu\text{W}$. Color scale is $(P_{\text{rad}}/P_{\text{fric}} - 1)$. Dashed black curve indicates unstable portion of contour. Red data points indicate initial (β_m, Δ_L) and grey data points indicate the final values, for selected instances of the experimental sequence as shown in (a). White arrows connect initial/final pairs but do not indicate the actual path taken by the system.

tal transduced power oscillates due to the nonlinearity of the detection process. All of these observations are nicely captured by our theoretical prediction (Fig. 2f, red curve). This has been obtained without fit parameters, except for an over-all scale factor in Fig. 2d. This agreement allows us to conclude that the oscillator is indeed traveling along the predicted paths through the attractor diagram shown in Fig. 2b.

It is readily apparent from Fig. 2a, that at large optical powers (black contour) there are a large number of isolated attractor contours at higher oscillation amplitudes. These attractors cannot be reached by slowly sweeping the detuning of the laser because the contours do not reach down to zero amplitude, nor can they be reached by noise, since the potential barriers are too high for the present parameters. However, external time-dependent driving of the mechanical mode allows us to access and explore the lowest-lying isolated attractor on the red side of the optical cavity ($\Delta_L < 0$), where the linearized theory predicts only damping of the mechanical mode.

To access this higher island, we use an EOM to phase-modulate the incoming light field. The resulting oscillating force inside the cavity drives the mechanical resonator towards higher amplitudes $\beta_m > 1$. In this driven regime, the external forcing induces injection-locking, i.e. the mechanical oscillator becomes synchronized to that of the drive. The result-

ing increase of oscillation amplitude can be exploited for control of the system dynamics. The experimental procedure is displayed in Fig. 3a, along with the corresponding gain spectrum and stable contours at the power used ($P_{\text{in}} = 43 \mu\text{W}$) is shown in Fig. 3b. We start with the pump laser switched on, but the phase modulation off, $\beta_{\text{EOM}} = 0$, at a detuning on the red side of the cavity resonance. Here, the laser acts to damp the mechanical resonator into a low-amplitude (cooled) thermal state: $\beta_m \approx 0$. Then, we switch on the EOM phase modulation, which rings up the mechanical resonator (shown in the time-domain inset of Fig. 3a). We now sweep the detuning to some starting value, Δ_L , completing the initialization sequence. Finally, we switch off the modulation ($\beta_{\text{EOM}} \rightarrow 0$) and record what final stable state the system relaxes into.

To get a measure of the mechanical oscillation amplitude, β_m , we send in an additional counter-propagating weak probe beam and scan it across the optical cavity to measure the cavity transmission spectrum during each period of the sequence as shown in the panels of Fig. 3d. When the mechanical amplitude is large ($\beta_m \gtrsim 1$) the standard single resonance dip of the optical cavity is transformed into a multi-featured spectrum symmetric about the cavity center with resonance dips of varying sizes near each mechanical sideband at $\Delta_p = \pm n\omega_m$. The varying relative amplitudes of these peaks allow us to pre-

cisely infer β_m without relying on calibration of the total detected power. We thus fit this spectrum to a theoretical curve calculated using Eq. 3 with β_m and ω_c as the free parameters (Fig. 3d, red curves). With our wavemeter independently establishing ω_L , from this fit we also know the true detuning of the drive laser, Δ_L (as opposed to using $\Delta_{L,0}$ as in Fig. 2).

We repeated this experimental procedure several times for different initial (β_m, Δ_L) states and recorded the resulting final states which reveal the flow in the underlying attractor diagram. A representative subset of the results are plotted in Fig. 3f. We find that after the modulation is switched off, for a narrow range of initial conditions, the system remains trapped close to the predicted top of the higher amplitude attractor at ($\beta_m \approx 3.5, \Delta_L/\omega_m \approx -0.7$). For more negative initial detunings or lower initial mechanical amplitudes, the system relaxes into the trivial low-amplitude state, or gets caught on the lowest-lying contour explored in Fig. 2. For detunings beyond $\Delta_L/\omega_m > -0.5$, the system could not be stably initialized due to thermo-optic effects.

The results presented here represent an initial exploration of the nonlinear attractor diagram of an optomechanical system where the dominant nonlinearity is that of the radiation pressure interaction. Due to the limited drive amplitude of the electro-optic modulator used in this work ($\beta_{\text{EOM}} \lesssim 3.5$), we are limited to exploring only the lowest red-side attractor. With the ability to apply larger drives, or to rapidly detune our laser, it should be possible to reach higher-lying islands, and more fully explore the attractor diagram shown in Fig. 2a. Further understanding of the latching effects in these measurements should also pave the way to exploiting them for use in metrology experiments. The dynamics that govern whether the oscillator stably latches into an attractor can be a very sensitive function of the oscillator's displacement [8], thus yielding a precise measurement of the oscillator's environment or state. This latching also allows for systems with memory due to the hysteretic nature of the nonlinearity, as in Ref. [21]. Such latching behavior has also been predicted [26] and observed in Josephson junctions [27, 28] and arrays of SQUIDs [29]. Finally, in future devices where the optomechanical coupling rate is larger, these same nonlinearities can lead to quantum mechanical effects which have thus far only been explored theoretically [30].

This work was supported by the DARPA ORCHID and MESO programs, the Institute for Quantum Information and Matter, an NSF Physics Frontiers Center with support of the Gordon and Betty Moore Foundation, the AFOSR through the “Wiring Quantum Networks with Mechanical Transducers” MURI program, and the Kavli Nanoscience Institute at Caltech. F.M. acknowledges an ERC Starting Grant OPTOMECH, ITN cQOM.

- Nature Photonics **6**, 768 (2012).
- [3] K. Srinivasan, H. Miao, M. T. Rakher, M. Davanco, and V. Aksyuk, Nano Letters **11**, 791 (2011).
 - [4] J. T. Hill, A. H. Safavi-Naeini, J. Chan, and O. Painter, Nature Communications **3**, 1196 (2012).
 - [5] A. H. Safavi-Naeini, S. Grblacher, J. T. Hill, J. Chan, M. Aspelmeyer, and O. Painter, Nature **500**, 185 (2013).
 - [6] Y. Chen, Journal of Physics B: Atomic, Molecular and Optical Physics **46**, 104001 (2013).
 - [7] W. Marshall, C. Simon, R. Penrose, and D. Bouwmeester, Physical Review Letters **91**, 130401 (2003).
 - [8] F. Marquardt, J. G. E. Harris, and S. M. Girvin, Physical Review Letters **96**, 103901 (2006).
 - [9] M. Eichenfield, R. Camacho, J. Chan, K. J. Vahala, and O. Painter, Nature **459**, 550 (2009).
 - [10] Q. Lin, J. Rosenberg, X. Jiang, K. J. Vahala, and O. Painter, Physical Review Letters **103**, 103601 (2009).
 - [11] A. H. Safavi-Naeini, T. P. M. Alegre, J. Chan, M. Eichenfield, M. Winger, Q. Lin, J. T. Hill, D. E. Chang, and O. Painter, Nature **472**, 69 (2011).
 - [12] S. Weis, R. Rivire, S. Delglise, E. Gavartin, O. Arcizet, A. Schliesser, and T. J. Kippenberg, Science **330**, 1520 (2010).
 - [13] J. Chan, T. P. M. Alegre, A. H. Safavi-Naeini, J. T. Hill, A. Krause, S. Grblacher, M. Aspelmeyer, and O. Painter, Nature **478**, 89 (2011).
 - [14] J. D. Teufel, T. Donner, D. Li, J. W. Harlow, M. S. Allman, K. Cicak, A. J. Sirois, J. D. Whittaker, K. W. Lehnert, and R. W. Simmonds, Nature **475**, 359 (2011).
 - [15] T. Carmon, H. Rokhsari, L. Yang, T. J. Kippenberg, and K. J. Vahala, Physical Review Letters **94**, 223902 (2005).
 - [16] H. Rokhsari, T. Kippenberg, T. Carmon, and K. Vahala, Optics Express **13**, 5293 (2005).
 - [17] T. J. Kippenberg, H. Rokhsari, T. Carmon, A. Scherer, and K. J. Vahala, Physical Review Letters **95**, 033901 (2005).
 - [18] K. Karrai, I. Favero, and C. Metzger, Physical Review Letters **100**, 240801 (2008).
 - [19] T. Carmon, M. C. Cross, and K. J. Vahala, Physical Review Letters **98**, 167203 (2007).
 - [20] C. Metzger, M. Ludwig, C. Neuenhahn, A. Ortlieb, I. Favero, K. Karrai, and F. Marquardt, Physical Review Letters **101**, 133903 (2008).
 - [21] M. Bagheri, M. Poot, M. Li, W. P. H. Pernice, and H. X. Tang, Nature Nanotechnology **6**, 726 (2011).
 - [22] J. Chan, A. H. Safavi-Naeini, J. T. Hill, S. Meenehan, and O. Painter, Applied Physics Letters **101**, 081115 (2012).
 - [23] M. Eichenfield, J. Chan, R. M. Camacho, K. J. Vahala, and O. Painter, Nature **462**, 78 (2009).
 - [24] T. P. M. Alegre, A. Safavi-Naeini, M. Winger, and O. Painter, Optics Express **19**, 5658 (2011).
 - [25] C. P. Michael, M. Borselli, T. J. Johnson, C. Chrystal, and O. Painter, Optics Express **15**, 4745 (2007).
 - [26] M. A. K. M. I. Dykman, Soviet Journal of Experimental and Theoretical Physics pp. 30– (1979).
 - [27] I. Siddiqi, R. Vijay, F. Pierre, C. M. Wilson, M. Metcalfe, C. Rigetti, L. Frunzio, and M. H. Devoret, Physical Review Letters **93**, 207002 (2004).
 - [28] I. Siddiqi, R. Vijay, F. Pierre, C. M. Wilson, L. Frunzio, M. Metcalfe, C. Rigetti, R. J. Schoelkopf, M. H. Devoret, D. Vion, et al., Physical Review Letters **94**, 027005 (2005).
 - [29] P. Jung, S. Butz, M. Marthaler, M. V. Fistul, J. Leppkangas, V. P. Koshelets, and A. V. Ustinov, Nature Communications **5** (2014).
 - [30] M. Ludwig, B. Kubala, and F. Marquardt, New Journal of Physics **10**, 095013 (2008).

[1] T. J. Kippenberg and K. J. Vahala, Science **321**, 1172 (2008).

[2] A. G. Krause, M. Winger, T. D. Blasius, Q. Lin, and O. Painter,